

24. Knoll, B. & Keilmann, F. Infrared conductivity mapping for nanoelectronics. *Appl. Phys. Lett.* **77**, 3980–3982 (2000).
25. Aravind, P. K. & Metiu, H. The effects of the interaction between resonances in the electromagnetic response of a sphere-plane structure; applications to surface enhanced spectroscopy. *Surf. Sci.* **124**, 506–528 (1983).
26. Shchegrov, A. V., Joulain, K., Carminati, R. & Greffet, J. J. Near-field spectral effects due to electromagnetic surface excitations. *Phys. Rev. Lett.* **85**, 1548–1551 (2000).
27. Hartmann, T., Kramer, A., Hillebrand, A., Guckenberger, R., et al. in *Procedures in Scanning Probe Microscopies* (ed. Colton, J. R.) 12–16 (Wiley, Chichester, 1998).
28. Aigouy, L. et al. Near-field optical spectroscopy using an incoherent light source. *Appl. Phys. Lett.* **76**, 397–399 (2000).

Acknowledgements

We acknowledge discussions with M. Stark, A. Otto, R. Helbig, R. Guckenberger and J. Plitzko. Supported by Deutsche Forschungsgemeinschaft.

Competing interests statement

The authors declare that they have no competing financial interests.

Correspondence and requests for materials should be addressed to E.K. (e-mail: keilmann@biochem.mpg.de).

Pressure-induced insulator-conductor transition in a photoconducting organic liquid-crystal film

Chong-yang Liu & Allen J. Bard

Department of Chemistry and Biochemistry, The University of Texas at Austin, Austin, Texas 78712, USA

Intermolecular separation determines the extent of orbital overlap and thus the rate of electron transfer between neighbouring molecules in an organic crystal. If such a crystal is compressed, the resistivity decreases owing to a diminishing intermolecular distance¹. Metal-insulator transitions have been observed by applying hydrostatic pressure to, for example, Langmuir films of metal nanoparticles^{2,3}. But previous attempts to observe a clear transition point in organic crystals, such as anthracene and tetracene, were not successful owing to difficulties with electrically insulating the high-pressure cell⁴. Here we report a different approach by using a sample that is photoconductive and forms an organized film. A cylindrical tip (~100 μm in diameter) was used to compress the sample instead of a piston/cylinder structure, entirely eliminating the problem of electrical insulation. Furthermore, by illuminating the sample with a laser, the conductivity of the sample is increased by several orders of magnitude. By monitoring the photocurrent with sensitivity at the 10⁻¹³ A level, changes in resistivity at very low pressure could be monitored. We observe a sharp increase in current that could indicate a transition from hopping to delocalized conduction.

Zinc octakis(β-decoxyethyl)porphyrin (ZnODEP) was used as the sample. In the crystal, molecules are regularly stacked to form well-defined molecular columns. As the intercolumn separation is large (~24 Å), each column is fairly isolated electronically from a neighbouring column^{5,6}. In fact, in the liquid-crystal state (95–147 °C), the column structure still remains in the discotic mesophase, although the long tails are disordered⁵. The molecule-to-molecule distance within the same column is also quite large (~4 Å). The structure of ZnODEP suggests that the solid should be relatively soft and easy to compress compared to other organic

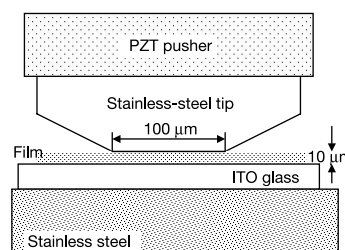


Figure 1 Schematic diagram of the experimental apparatus. A PZT pusher capable of moving extremely slowly (a few Å s⁻¹) was used to drive the tip so that the sample could be maintained in a quasi-equilibrium state during compression. A balance (Sartorius, 1212 MP) was used to measure the pressure precisely by placing the sample on its top.

crystals, such as anthracene. Films were made by a capillary filling of the substance in the molten state into empty ITO (indium tin oxide) sandwich cells as reported earlier^{7,8}. The cells were then cooled to form a solid film, and separated to produce a free surface. As shown in previous work^{7–9}, the axes of the molecular columns are oriented perpendicular to the ITO surface, so that the pressure would mainly affect the intermolecular interactions within the same columns.

An argon-ion laser (100 mW at 488 nm, Melles Griot) was used to irradiate the film via a fibre optic through the ITO glass. The tip was made from a stainless-steel cylinder about 0.1 inch in diameter with one end tapered to a sharp point by mechanical polishing. The tip was then pressed against a stainless-steel or glass plate to flatten the end to about 100–150 μm diameter by applying very high pressure. The overall structure is tip/film/ITO (Fig. 1). The electrical contacts were made to both the ITO and the tip electrodes. The tip was pushed by a PZT (lead zirconate titanate) pusher (Burleigh) to compress the film. A micrometer was attached to the other end of the pusher for the initial rough adjustment of the distance between the tip and the film.

When the tip was brought into contact with the ZnODEP film, a steady photocurrent was observed under a fixed bias voltage of 3.2 V (with the tip negative). The magnitude of the photocurrent depended on the initial film thickness. A short-circuit photocurrent could also be detected, as reported earlier, with large-area ITO/ZnODEP/ITO sandwich cells^{9–11}. This current is produced by preferential injection of photogenerated electrons from ZnODEP molecules into the illuminated ITO electrode, while holes hop through the film to the tip electrode. Note that the photocurrent started to increase immediately following the tip's forward move-

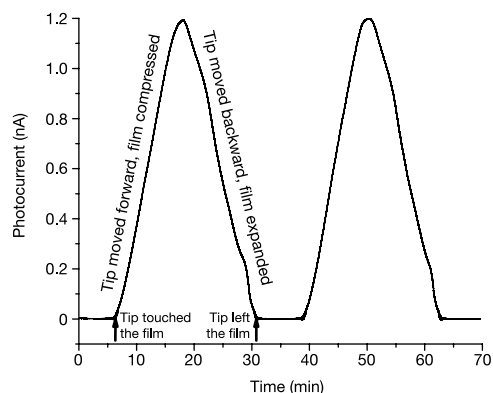


Figure 2 Photocurrent as a function of compression and expansion of a ZnODEP film about 6 μm thick between ITO glass and a stainless-steel tip. The ITO glass was placed on a fixed stainless-steel platform, and the tip was moved at a rate of 4 nm s⁻¹. The film was irradiated from the ITO side with a fibre optic through a hole in the platform. A bias voltage of 3.2 V was applied between sample and tip, with the tip negative.

ment to compress the film, and linearly increased from subpicoamp to nanoamp levels during the film compression. When the light was cut off briefly from time to time, the photocurrent dropped by several orders of magnitude, as expected, and increased back to the same level when the light was turned on again. When the film had been compressed to a certain level and the tip was then moved backward so that the film expanded, the photocurrent decreased. Reversible changes in photocurrent were observed during cycles of film compression and expansion (Fig. 2). The tip could be moved back and forth for many cycles at the same spot without affecting the reversibility and the magnitude of the photocurrent, indicating that the film beneath the tip was quite flexible and not physically damaged. Examination of the film under an optical microscope after the experiment showed no indentation or other damage at the position where the tip compression occurred, confirming that the applied pressure was mainly confined to an area over the molecular columns.

When the film was compressed further, a point was reached where the slope of the log current versus displacement curve greatly increased and the current became larger by several orders of magnitude (Fig. 3). A photocurrent at the 0.1 μA level was obtained, which was over six orders of magnitude higher than the initial value. This increase can be explained by a decrease in the intermolecular separation to such a level that the molecular orbitals overlap, changing the charge carrier transport mechanism from hopping to delocalized conduction. We do not know the pressure distribution along the molecular columns from the tip to the ITO substrate. Perhaps molecular separations near the tip were first decreased by compression at low pressure, while the intermolecular distances near the ITO surface were decreased at the critical pressure, leading to a very marked increase in current (Fig. 3). On the other hand, the molecular distances might be decreased relatively uniformly. In either case, however, the sharp current increase would signal a transition from hopping to delocalized conduction. We are not aware of any theory predicting such a transition.

The estimated resistivity of the ZnODEP film beneath the tip was of the order of $10^6 \Omega \text{ cm}$, indicating that the insulator was changed into a semiconductor. The pressure at the transition point was about 2.2 kbar, as determined with a balance (176 g over a tip about $100 \mu\text{m}$ in diameter). Seven measurements at different locations on the film showed the same result. Careful examination under an

optical microscope indicated that the shape of the tip was not changed after these measurements. Once the material became a semiconductor under pressure, the current was a function of bias voltage (Fig. 4). This current–voltage curve was very stable: ten consecutive curves essentially overlapped. The nonlinear behaviour clearly indicates that the tip was not in direct contact with the ITO substrate. In fact, the compressed film under the tip was still about $6 \mu\text{m}$ thick.

The same general behaviour was found for the film in the dark (Fig. 3). The initial current was over two orders of magnitude smaller, but a transition to a more conductive state was seen at essentially the same pressure as that for the illuminated film. Moreover, the optical properties of the ZnODEP film under pressure also changed when the compression was carried out on the stage of an inverted optical microscope (Nikon, TE300). The red colour of the film became darker with increasing pressure. Additional studies of the optical effects of compression are planned.

To determine how much the films were compressed under the tip, the samples were placed on a fixed stainless-steel platform instead of the balance. Before each measurement, the tip was directed first to the bare ITO surface next to the ZnODEP film. Once a tunnelling current between the tip and ITO was detected, the tip was withdrawn a known distance. The tip was then moved to approach the film and start the compression while the current and travel distance of the tip were monitored continuously. After the measurement, tip was moved to bare ITO surface again to assess the distance. This measured distance was exactly the same, even after the sample was taken out and put back onto the platform a number of times. Thus, the changes in the film thickness during the compression could be calculated. There is some uncertainty, however, because other parts, including the ITO glass, could be compressed to some degree. Because the glass and stainless steel are much harder than the ZnODEP film, their compression is probably negligible. The data indicate that the film was compressed by about 50% at the transition point. This can be compared to the 30–40% shrinkage observed with aromatic crystals, such as pentacene, at a pressure in the region of several hundred kilobars¹².

As mentioned above, the ZnODEP material is relatively soft owing to its structure (Fig. 3 inset), and is very different from conventional organic molecular crystals. Indeed, when anthracene films ($\sim 10 \mu\text{m}$ thick) were tested with our apparatus, the transition point was not seen under a pressure beyond our balance's upper

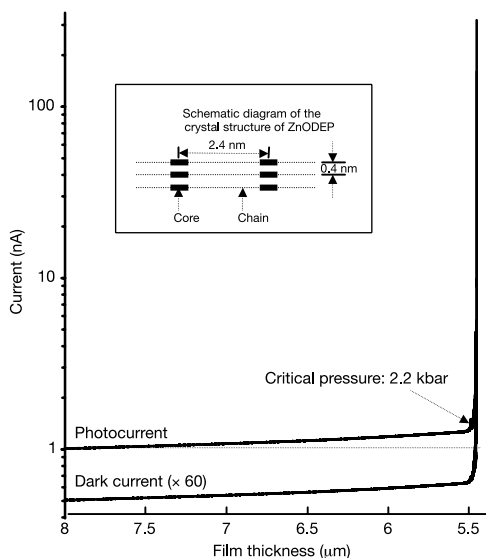


Figure 3 Photocurrent as a function of distance during the compression of a ZnODEP film about $10 \mu\text{m}$ thick between ITO glass and a stainless-steel tip. A bias voltage of 3.2 V was applied to the sample with the tip negative, and the film was compressed at a rate of 4 nm s^{-1} . Inset, schematic structure of ZnODEP.

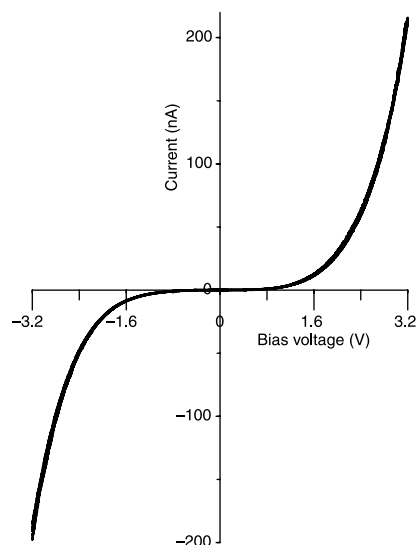


Figure 4 Current as a function of bias voltage in ZnODEP semiconductor (pressure about 2.7 kbar). Ten consecutive curves overlapped. Scan rate, 50 mV s^{-1} . The photocurrent was at 10^{-13} A under a bias voltage of 3.2 V when there was no compression.

limit, which was twice as high as the transition pressure for ZnODEP. □

Received 12 February; accepted 27 May 2002; doi:10.1038/nature00875.

1. Drickamer, H. G. & Frank, C. W. Electronic structure, electronic transitions, and the high pressure chemistry and physics of solids. *Annu. Rev. Phys. Chem.* **23**, 39–64 (1972).
2. Collier, C. P., Saykally, R. J., Shiang, J. J., Henrichs, S. E. & Heath, J. R. Reversible tuning of silver quantum dot monolayers through the metal-insulator transition. *Science* **277**, 1978–1981 (1997).
3. Henrichs, S., Collier, C. P., Saykally, R. J., Shen, Y. R. & Heath, J. R. The dielectric function of silver nanoparticle Langmuir monolayers compressed through the metal insulator transition. *J. Am. Chem. Soc.* **122**, 4077–4083 (2000).
4. Samara, G. A. & Drickamer, H. G. Effect of pressure on the resistance of fused-ring aromatic compounds. *J. Chem. Phys.* **37**, 474–479 (1962).
5. Liu, C.-Y., Pan, H.-L., Tang, H., Fox, M. A. & Bard, A. J. Effect of structural order on the dark and photocurrents in zinc octakis (β -deoxyethyl)porphyrin thin-layer cells. *J. Phys. Chem.* **99**, 7632–7636 (1995).
6. Schouten, P. G., Warman, J. M., de Haaas, M. P., Fox, M. A. & Pan, H.-L. Charge migration in supramolecular stacks of peripherally substituted porphyrins. *Nature* **353**, 736–737 (1991).
7. Liu, C.-Y. & Bard, A. J. Optoelectronic properties and memories based on organic single-crystal thin films. *Acc. Chem. Res.* **32**, 235–245 (1999).
8. Liu, C.-Y. & Bard, A. J. in *Conjugated Oligomers, Polymers, and Dendrimers: From Polyacetylene to DNA* (ed. Brédas, J.-L.) 85–116 (De Boeck Université, Paris, 1999).
9. Gregg, B. A., Fox, M. A. & Bard, A. J. Photovoltaic effect in symmetrical cells of a liquid crystal porphyrin. *J. Phys. Chem.* **94**, 1586–1598 (1990).
10. Liu, C.-Y. & Bard, A. J. Optoelectric charge trapping/detrapping in thin solid films of organic azo dyes: Application of scanning tunneling microscopic tip contact to photoconductive films for data storage. *Chem. Mater.* **10**, 840–846 (1998).
11. Liu, C.-Y., Pan, H.-L., Fox, M. A. & Bard, A. J. Reversible charge trapping/detrapping in a photoconductive insulator of liquid crystal zinc porphyrin. *Chem. Mater.* **9**, 1422–1429 (1997).
12. Aust, R. B., Bentley, W. H. & Drickamer, H. G. Behavior of fused-ring aromatic hydrocarbons at very high pressure. *J. Chem. Phys.* **41**, 1856 (1964).

Acknowledgements

We thank F.-R.F. Fan for discussions. This work was supported by the National Science Foundation and the Robert A. Welch Foundation.

Competing interests statement

The authors declare that they have no competing financial interests.

Correspondence and requests for materials should be addressed to A.J.B. (e-mail: ajbard@mail.utexas.edu).

Self-regeneration of a Pd-perovskite catalyst for automotive emissions control

Y. Nishihata*, J. Mizuki*, T. Akao*†, H. Tanaka‡, M. Uenishi‡, M. Kimura§, T. Okamoto†§ & N. Hamada||

* Synchrotron Radiation Research Center, Japan Atomic Energy Research Institute, Mikazuki, Sayo-gun, Hyogo 679-5148, Japan

‡ Materials R&D Division, Technical Center, Daihatsu Motor Co. Ltd, Ryuo, Gamo-gun, Shiga 520-2593, Japan

§ Materials Analysis & Evaluation Division, Toyota Central R&D Laboratories Inc., Nagakute, Aichi-gun, Aichi 480-1192, Japan

|| Faculty of Science and Technology, Tokyo University of Science, Noda, Chiba 278-8510, Japan

Catalytic converters are widely used to reduce the amounts of nitrogen oxides, carbon monoxide and unburned hydrocarbons in automotive emissions. The catalysts are finely divided precious-metal particles dispersed on a solid support. During vehicle use, the converter is exposed to heat, which causes the metal particles to agglomerate and grow, and their overall surface area to decrease. As a result, catalyst activity deteriorates. The

problem has been exacerbated in recent years by the trend to install catalytic converters closer to the engine, which ensures immediate activation of the catalyst on engine start-up, but also places demanding requirements on the catalyst’s heat resistance. Conventional catalyst systems thus incorporate a sufficient excess of precious metal to guarantee continuous catalytic activity for vehicle use over 50,000 miles (80,000 km). Here we use X-ray diffraction and absorption to show that $\text{LaFe}_{0.57}\text{Co}_{0.38}\text{Pd}_{0.05}\text{O}_3$, one of the perovskite-based catalysts investigated^{1–4} for catalytic converter applications since the early 1970s, retains its high metal dispersion owing to structural responses to the fluctuations in exhaust-gas composition that occur in state-of-the-art petrol engines⁵. We find that as the catalyst is cycled between oxidative and reductive atmospheres typically encountered in exhaust gas, palladium (Pd) reversibly moves into and out of the perovskite lattice. This movement appears to suppress the growth of metallic Pd particles, and hence explains the retention of high catalyst activity during long-term use and ageing.

A state-of-the-art automotive petrol engine is operated close to the stoichiometric air-to-fuel ratio (by using an oxygen sensor and a sophisticated feedback control system linked to the catalyst) in order to convert simultaneously three pollutant emissions—carbon monoxide (CO), hydrocarbons, and nitrogen oxides (NO_x)²—into carbon dioxide (CO_2), water (H_2O) and nitrogen (N_2). A time lag associated with adjusting the air-to-fuel ratio results in a redox fluctuation in the exhaust gas. We designed our catalyst system to react to this fluctuation, to achieve greater efficiency and to conserve precious metals.

The conversion of CO and NO_x is equal at the CO– NO_x cross-over point (see Methods for catalytic evaluation), and the conversion at this point is generally accepted as a useful indicator of catalytic activity⁶. Figure 1 compares the activity of two catalysts using this indicator; one is $\text{LaFe}_{0.57}\text{Co}_{0.38}\text{Pd}_{0.05}\text{O}_3$ (Pd-perovskite, our ‘intelligent’ catalyst), and the other is Pd-impregnated $\gamma\text{-Al}_2\text{O}_3$ (Pd/alumina, the conventional catalyst; see Methods for catalyst preparation and testing). The Pd-perovskite catalyst maintains its high activity during ageing, whereas the activity of the Pd/alumina catalyst deteriorates by about 10%. (See Supplementary Information Fig. 1 for details on the conversion of different pollutants during the sweep test.) Imaging of the aged catalysts by transmission electron microscopy showed that the Pd particles on alumina reached sizes of up to 120 nm, whereas only small metallic particles about 1–3 nm in diameter were found on the perovskite surface (see Supplementary Information Fig. 2). X-ray energy dispersion analysis indicated that the small particles contain not only Pd, but also

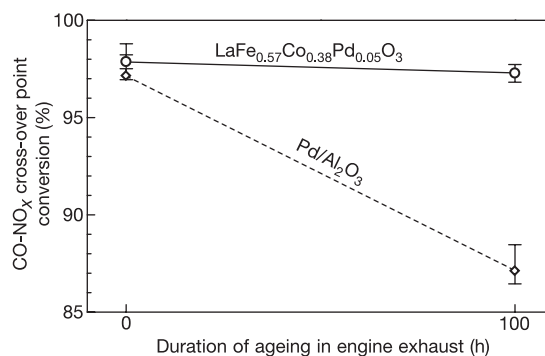


Figure 1 Change in catalyst activity during ageing. Shown is the ageing dependence of the CO– NO_x cross-over point conversion for $\text{LaFe}_{0.57}\text{Co}_{0.38}\text{Pd}_{0.05}\text{O}_3$ (Pd-perovskite catalyst) and Pd-impregnated $\gamma\text{-Al}_2\text{O}_3$ (Pd/alumina catalyst). The conversion efficiency was evaluated three times for each sample by the sweep test (see Methods). The median of the CO– NO_x cross-over point conversion (see Methods) is plotted as the symbol, together with the maximum and the minimum as error bars.

† Present addresses: Faculty of Engineering, Tottori University, Tottori 680-8552, Japan (T.A.); Research Institute for Science and Technology, Chubu University, Kasugai, Aichi 487-8501, Japan (T.O.).